

Supporting Information

Highly Sensitive and Stable SERS Substrate Using Hybrid Tungsten

Dioxide/Carbon Ultrathin Nanowire Beams

Chenying He^a, Hua Bai^a, Wencai Yi^b, Jingyao Liu^b, Xinshi Li^a, Xia Li^c, and
Guangcheng Xi^{a*}

^a Institute of Industrial and Consumer Product Safety Institution Chinese Academy of
Inspection and Quarantine, No. 11, Ronghua South Road, Beijing 100176, P. R. China.

^b Institute of Theoretical Chemistry, Jilin University, No. 2699, Qianjin Street,
Changchun 130023, P. R. China.

^c Department of Chemistry, Capital Normal University, No. 105, North Road, West 3th
Ring Road, Beijing, 100048, P. R. China.

Experimental Section

Synthesis of Carbon Fibres

0.5 g of WO₂/C ultrathin nanowire beams was added into 200 mL of H₂SO₄ solution (10 M). The mixed solution was heated to 60 °C and kept for 5 hours under agitation. Finally, the black products were collected, purified with absolute ethanol and distilled water, and dried in air at 50 °C.

Calculation of EFs

To calculate the EF of the WO₂/C ultrathin nanowire beams, the ratio of SERS to normal Raman spectra (NRS) of R6G was determined by using the following calculating formula 1

$$EF = (I_{SERS}/N_{SERS})/(I_{NRS}/N_{NRS}) \quad (1)$$

$$N_{SERS} = N_A n S_{Irr}/S_{dif} \quad (2)$$

$$N_{NRS} = d S_{Irr} h N_A / M \quad (3)$$

where I_{SERS} and I_{NRS} refer to the peak intensities of the SERS and NRS, respectively.

N_{SERS} and N_{NRS} correspond to the number of probe molecules excited in the SERS and NRS tests. In the SERS measurements, Raman scattering peak, R_1 at 612 cm⁻³ was selected for the calculations of the EF. For comparison, the peak intensities of the R6G (1×10^{-2} M, aqueous solution) directly placed on bare glass were detected as NRS data.

To decrease the measuring error, the intensities were obtained by continually ran the test procedure at randomly selected 50 points and took the average. N_{SERS} is calculated by formula 2, where N_A refer to the Avogadro's constant, n correspond to the molar quantity of the probe molecule, S_{Irr} refer to the irradiation area under the laser beam (5

m in diameter), and S_{dif} refer to the diffusion area of the substance to be tested on the substrate. In a typical test, one drop (20 microliter) of the probe solution was dropped onto the SERS substrate, and the probe solution was spread into a circle with a diameter of 4 mm when the solution is completely dry. N_{NRS} is determined by the formula 3, where d is the packing density of R6G molecules in the surface of substrate (1.4×10^{21} molecule/cm³), h refer to the laser confocal depth (26 μm), M correspond to the molecule weight of R6G (479).

Electronic Structure Calculations

The density functional theory based calculations are carried out by the Vienna ab initio Simulation Package (VASP), within the projector-augmented-wave approach.^[1-4] And the generalized gradient approximation (GGA) with the function of Perdew and Wang (PW91) was employed for the exchange correlation functional,^[5-6] where the W-5d⁴6s² states and the O-2s²2p⁴ states were treated as valence states. The cutoff energy was chosen at value of 600eV, Brillouin zones (BZ) integrations were carried using Monkhorst-Pack sampling grids^[7] with resolution of $2\pi \times 0.2 \text{ \AA}^{-1}$ and $2\pi \times 0.1 \text{ \AA}^{-1}$ for structure optimizations and DOS calculations, respectively. The high symmetry path was determined by materials tools.^[8] The atomic positions and lattice constants were optimized using the conjugate gradients (CG) scheme until the force components on each atom were less than 0.02 eV/Å. All the electronic structure calculations were calculated by hybrid functional (HSE06). Both monoclinic phase WO₃ (space group P21/c) and WO₂ (space group P21/c) were modeled in our calculations and the optimized lattice parameters were $a=5.59, b=4.94, c=5.71 \text{ \AA}$, $\alpha=\gamma=90^\circ$, $\beta=120.48^\circ$ for

WO₂ and $a = 7.52$, $b = 7.71$, $c = 7.85$ Å, $\alpha = \gamma = 90^\circ$, $\beta = 90.18^\circ$ for WO₃, which agree well with the previous experimental and calculation results.^[1, 9-10]

Reference

- [1] F. H. Jones, R. G. Egdell, A. Brown, F. R. Wondre, *Surf. Sci.* **1997**, 374, 80-94.
- [2] G. Kresse, J. Hafner, *Phys. Rev. B* **1994**, 49, 14251-14269.
- [3] G. Kresse, J. Furthmüller, *Comp. Mater. Sci.* **1996**, 6, 15-50.
- [4] G. Kresse, J. Furthmüller, *Phys. Rev. B* **1996**, 54, 11169-11186.
- [5] J. P. Perdew, K. Burke, M. Ernzerhof, *Phys. Rev. Lett.* **1996**, 77, 3865-3868.
- [6] G. Kresse, D. Joubert, *Phys. Rev. B* **1999**, 59, 1758-1775.
- [7] H. J. Monkhorst, J. D. Pack, *Phys. Rev. B* **1976**, 13, 5188-5192.
- [8] Y. Hinuma, G. Pizzi, Y. Kumagai, F. Oba, I. Tanaka, *Comp. Mater. Sci.* **2017**, 128, 140-184.
- [9] G. A. Niklasson, C. G. Granqvist, *J. Mater. Chem.* **2007**, 17, 127-156.
- [10] D. B. Migas, V. L. Shaposhnikov, V. E. Borisenko, *J. Appl. Phys.* **2010**, 108, 093714.

Figures

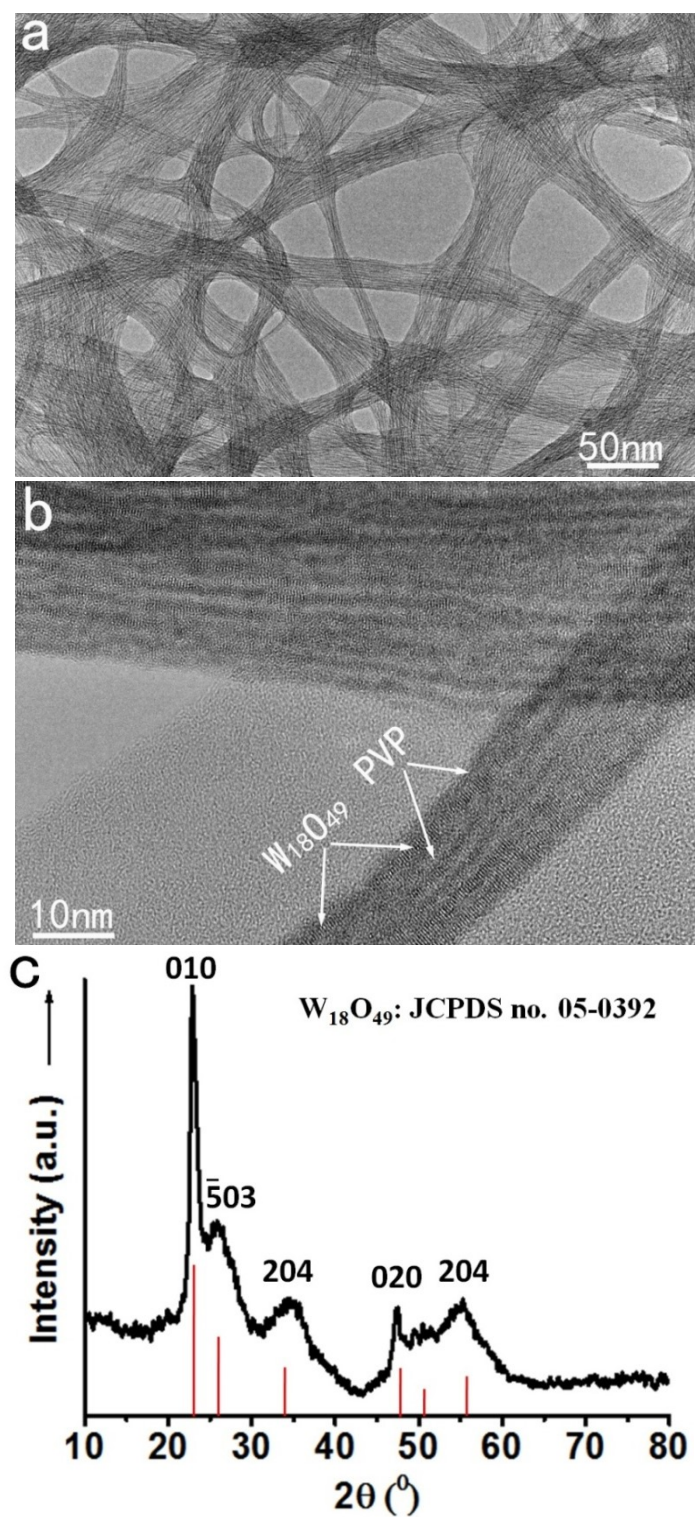


Figure S1. Morphology, structure, and crystal phase characterizations of the $W_{18}O_{49}$ /PVP ultrathin nanowire beams: (a) TEM image; (b) HRTEM image; (c) XRD pattern.

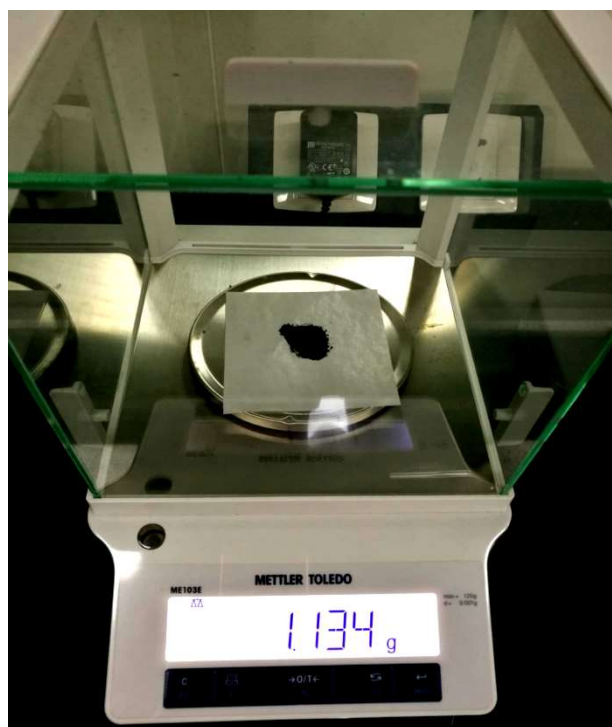


Figure S2. The WO_2/C UNBs can of g-scale by this simple reaction route.

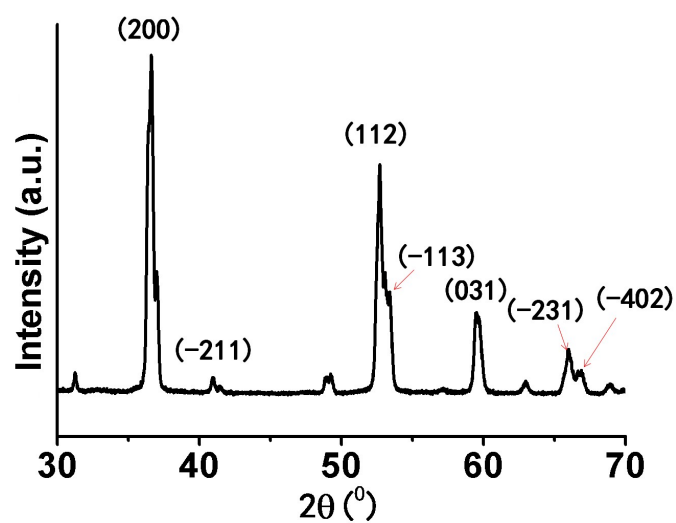


Figure S3. XRD pattern of the as-synthesized WO₂/C ultrathin nanowire beams by heating W₁₈O₄₉/PVP ultrathin nanowire beams in N₂.

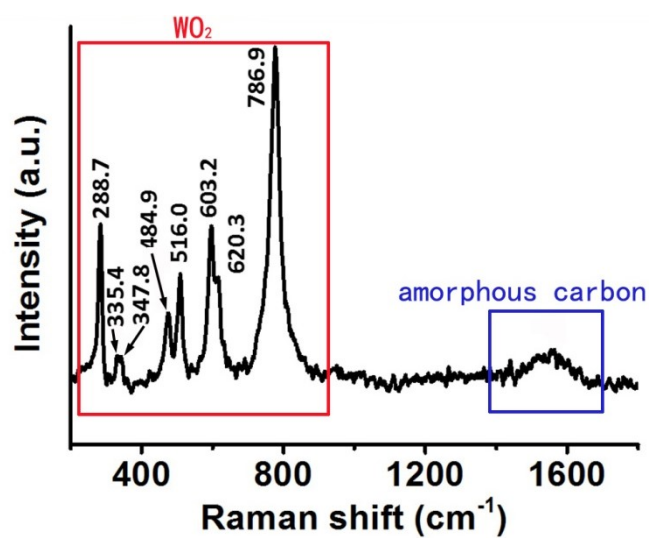


Figure S4. Raman spectrum of the WO₂/C ultrathin nanowire beams. This spectrum clearly demonstrates that the WO₂ nanowires are highly crystalline, while the carbon layers are amorphous carbon.

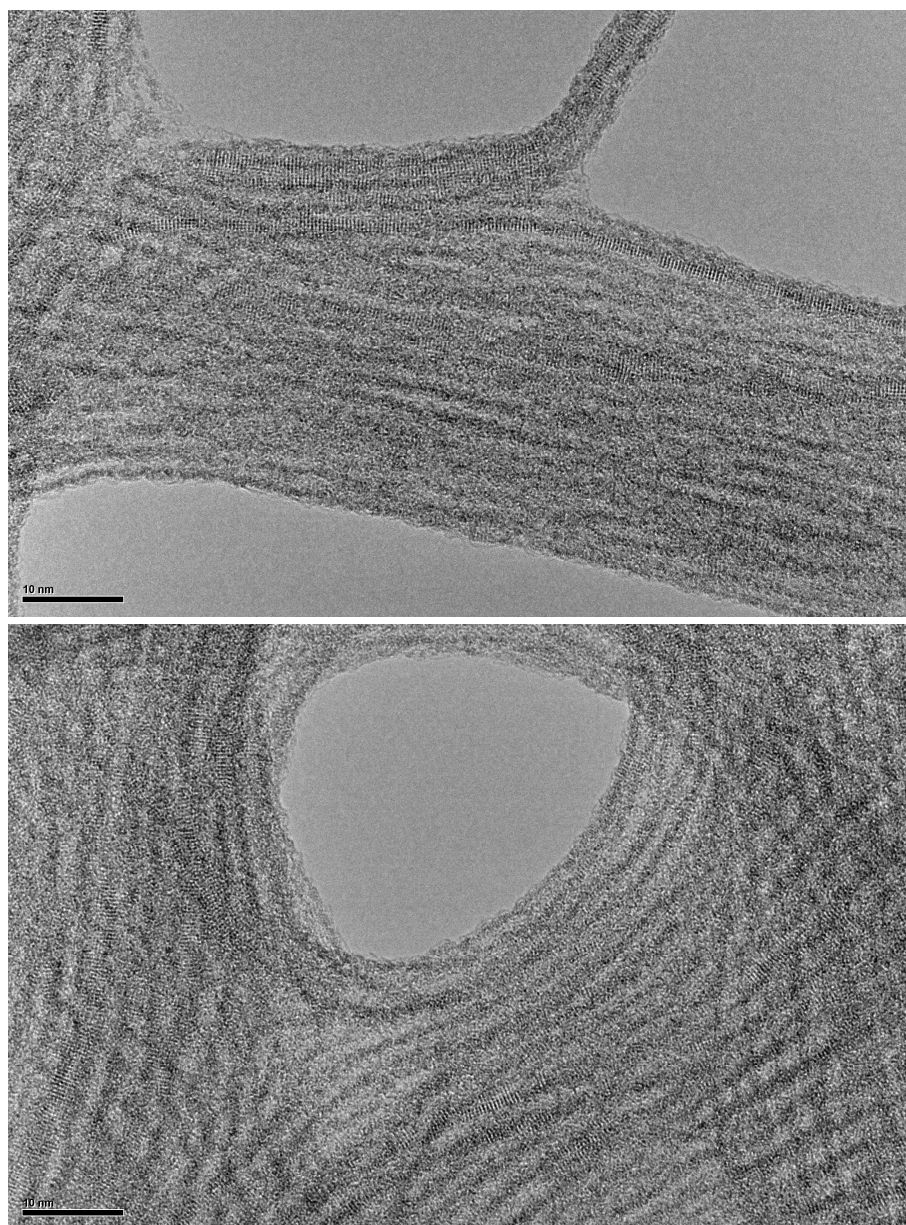


Figure S5. Additional HRTEM images of the obtained WO₂/C ultrathin nanowire beams, which can be seen that the WO₂ nanowires are highly crystalline and the carbon layers are amorphous.

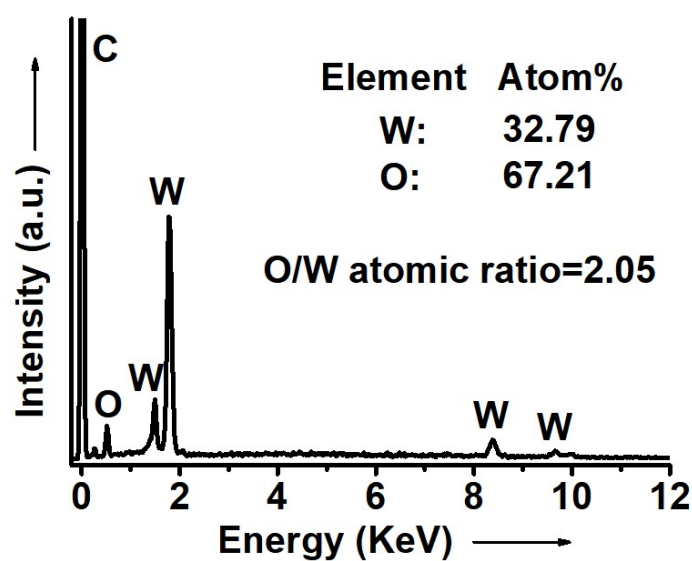


Figure S6. EDS component analysis of the WO₂/C ultrathin nanowire beams.

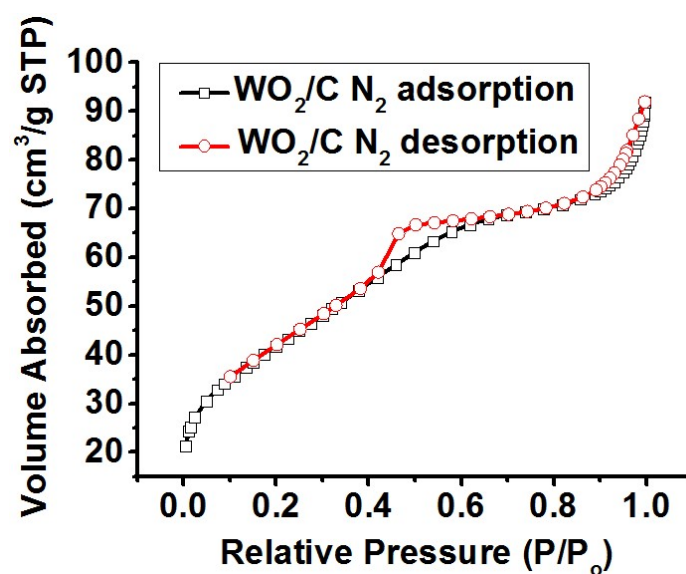


Figure S7. N₂ adsorption/desorption isotherms of the as-synthesized WO₂/C ultrathin nanowire beams, which shows the WO₂/C ultrathin nanowire beams have a large specific surface area of 101.5 m² g⁻¹.

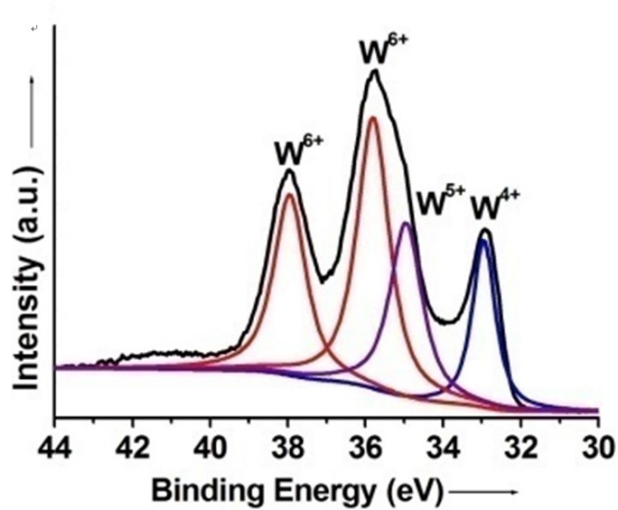


Figure S8. XPS of the WO_2/C ultrathin nanowire beams. In the spectra, the peaks located at 32.9 and 34.8 eV can be indexed into the W^{4+} and W^{5+} respectively, while the peaks located at 35.8 and 37.9 eV can be indexed into W^{6+} . These W^{6+} and W^{5+} atoms are derived from oxidized W atoms on the surface of the WO_2 nanowires. Because the diameter of the nanowires is only about 1 nm, and the detection depth of XPS is up to 2-3 nm, the ratios of W^{6+} and W^{5+} atoms is relatively high.

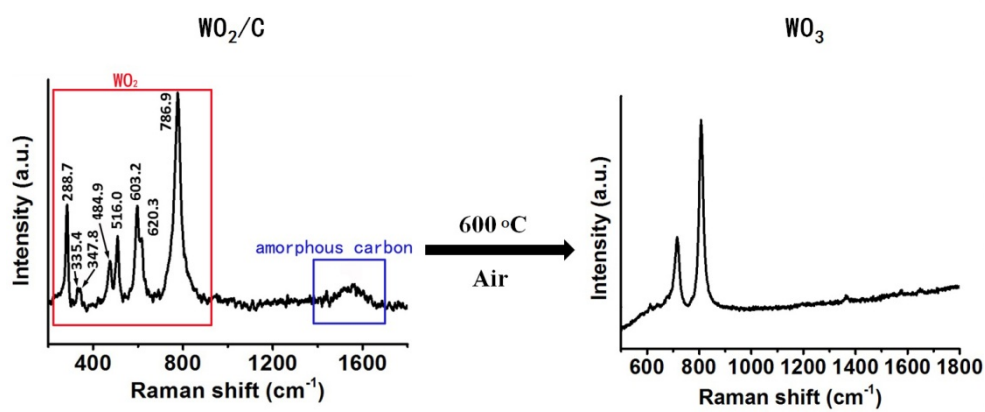


Figure S10. The structure evolution from WO_2/C to WO_3 can be reflected by the Raman spectra changes.

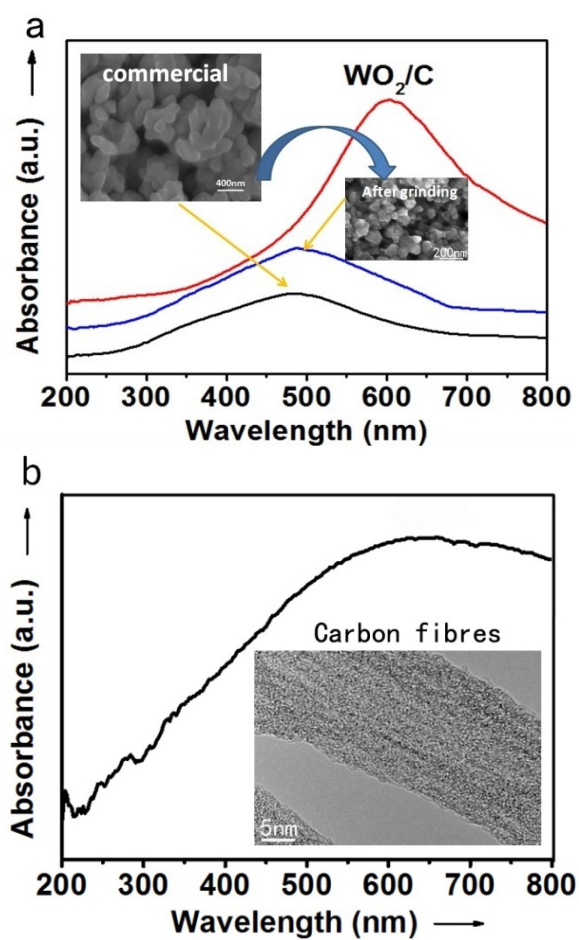


Figure S11. The UV-Vis spectra of the WO_2/C ultrathin nanowire beams, commercial WO_2 powders (a) , and the carbon fibres obtained by removing the WO_2 from the WO_2/C ultrathin nanowire beams (b). Inset in Figure S11a: SEM image of the commercial WO_2 powders; Inset in Figure S11b: SEM image of the carbon fibres.

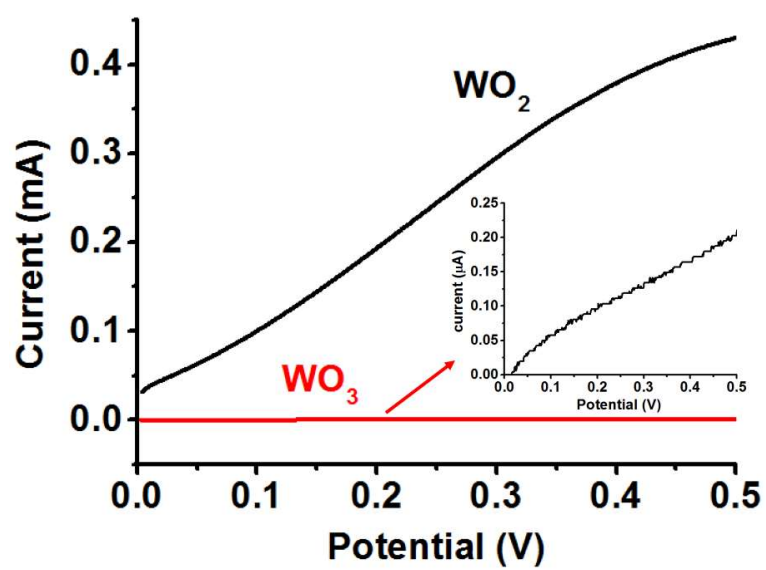


Figure S12. photocurrent spectra of the WO_2/C ultrathin nanowire beams and the chain-like WO_3 nanowires.

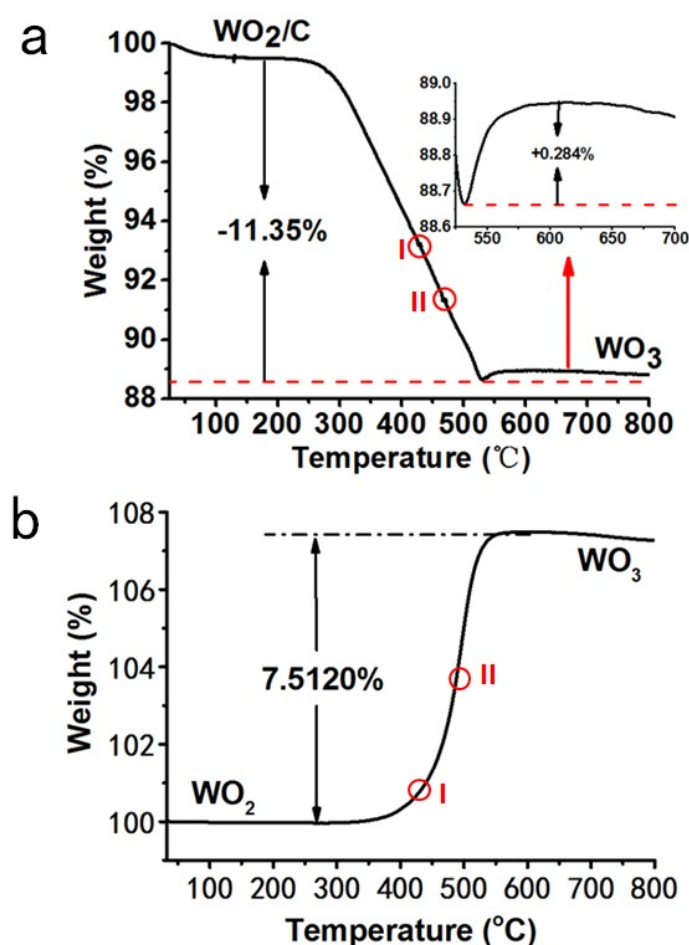


Figure S13. (a) Differential thermal analysis (DTA) of the WO_2/C UNBs. (b) DTA of the commercial WO_2 powders.

Note: because of the strong interference of carbon in the analysis process of the WO_2/C UNBs, we chose commercial pure WO_2 as the reference sample. In Figure S16a, it is evident that there are fluctuations in the two regions (I and II) of the weightless trend line. Compared with the Figure S16b, it can be found that the two fluctuation regions shown in Figure S16a correspond to the oxidation threshold temperature and the fast transition temperature of pure WO_2 . Combined with the two figures, it can reasonably conclude that the starting temperature of WO_2 ultrafine nanowires transformed to WO_3 is about 400 $^{\circ}\text{C}$. The weight gain during the transition (from WO_2 to WO_3) is mostly neutralized by the loss of carbon contained in the WO_2/C UNBs.

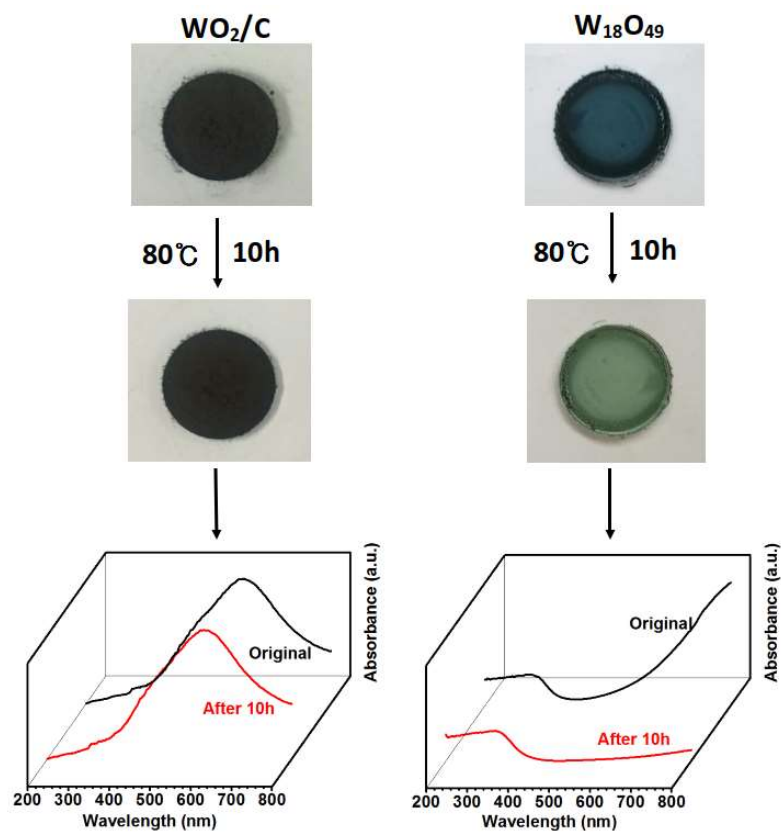


Figure S14. Comparison of oxidation resistance of WO_2/C ultrathin nanowire beams and $\text{W}_{18}\text{O}_{49}$ nanowires: these results clearly demonstrate that WO_2/C has much higher antioxidant activity than $\text{W}_{18}\text{O}_{49}$.

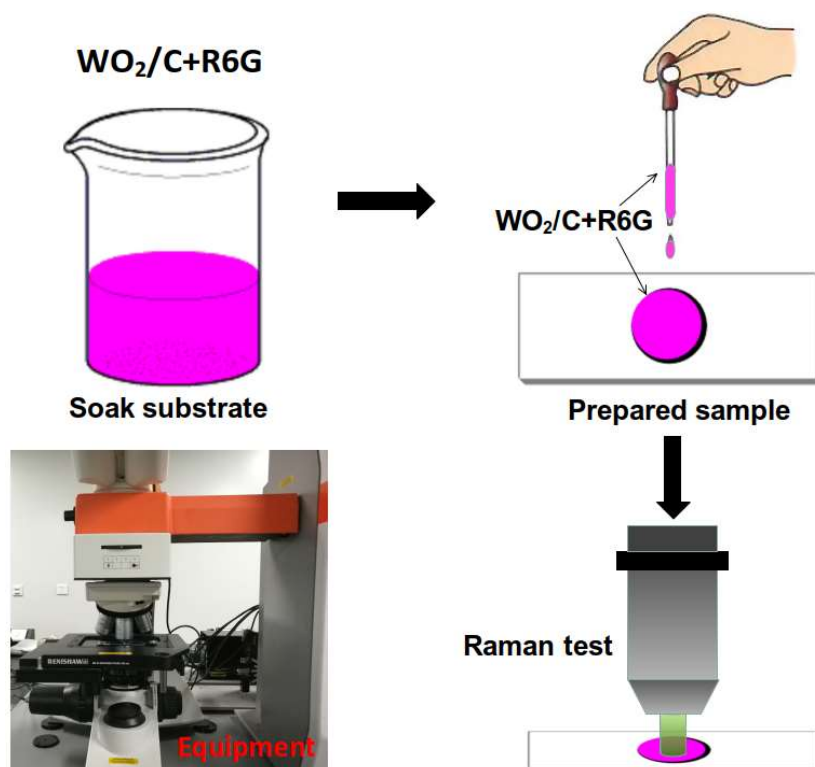


Figure S15. The substrate preparation and sample test process.

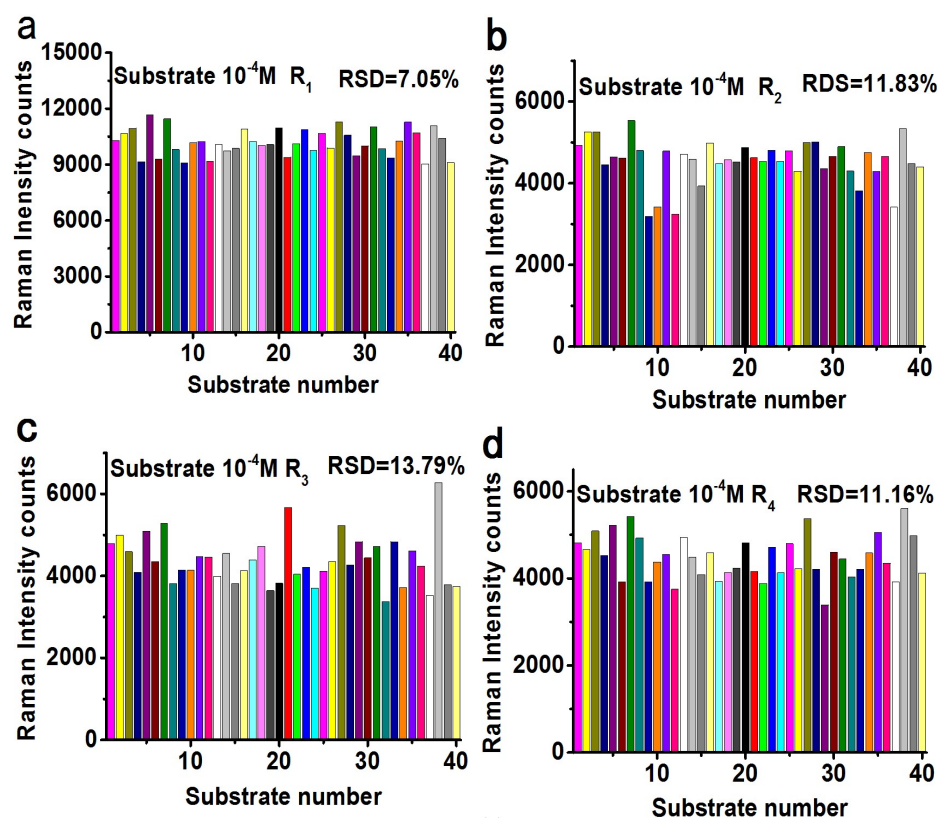


Figure S16. Relative standard deviation (RSD) of statistically obtained from more WO_2/C substrates by using the intensities of R_1 , R_2 , R_3 , and R_4 at 10^{-4} M. For each concentration, a total of 40 intensity values were collected from one WO_2/C substrate.

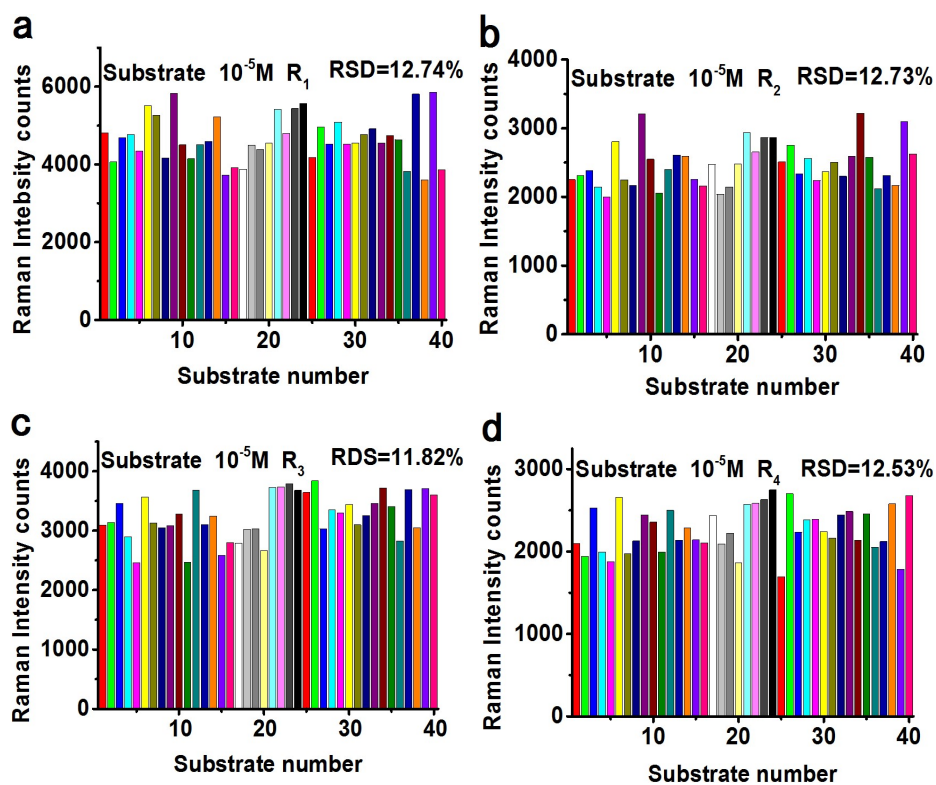


Figure S17. Relative standard deviation (RSD) of statistically obtained from more WO₂/C substrates by using the intensities of R₁, R₂, R₃, and R₄ at 10^{-5} M. For each concentration, a total of 40 intensity values were collected from one WO₂/C substrate.

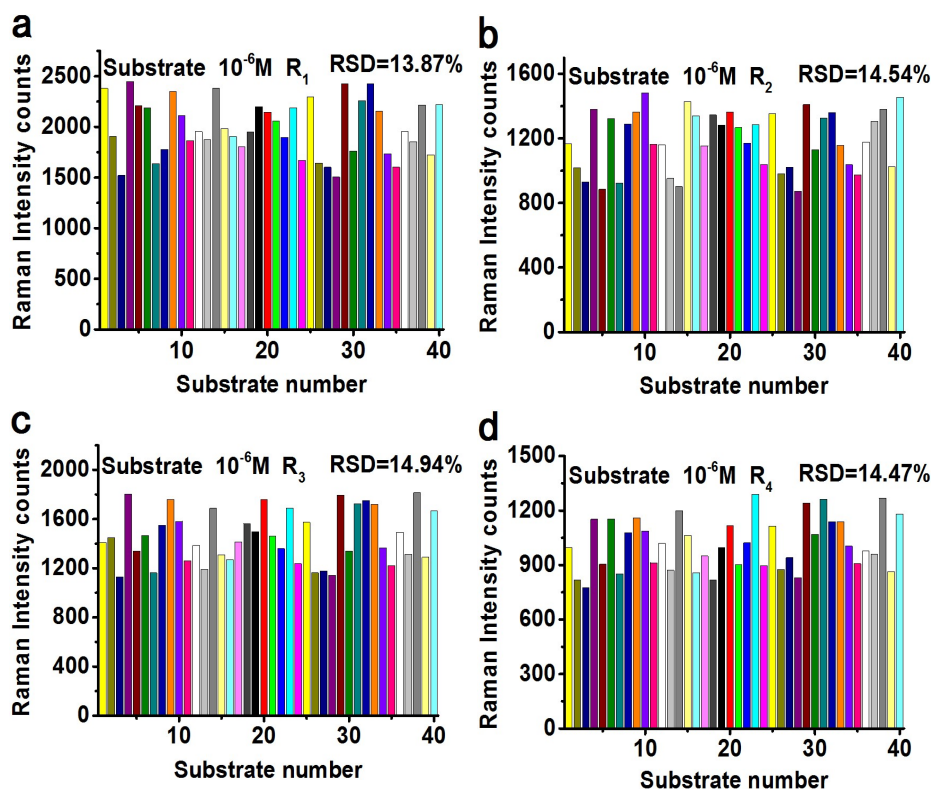


Figure S18. Relative standard deviation (RSD) of statistically obtained from more WO_2/C substrates by using the intensities of R_1 , R_2 , R_3 , and R_4 at 10^{-6} M. For each concentration, a total of 40 intensity values were collected from one WO_2/C substrate.

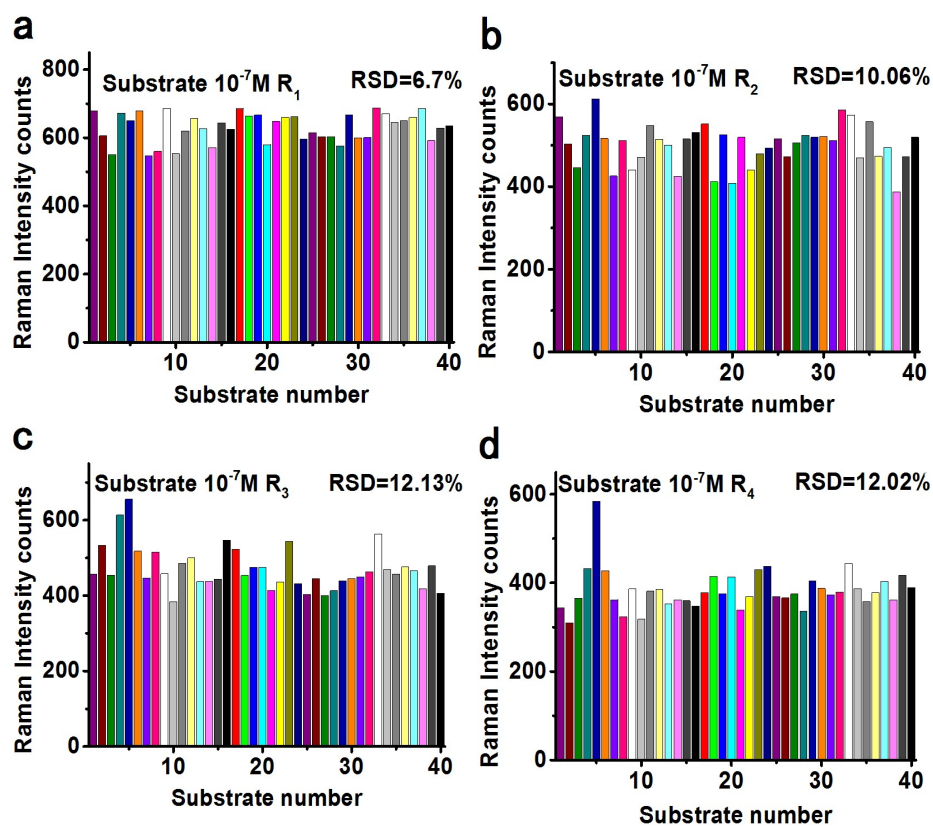


Figure S19. Relative standard deviation (RSD) of statistically obtained from more WO_2/C substrates by using the intensities of R_1 , R_2 , R_3 , and R_4 at 10^{-7} M. For each concentration, a total of 40 intensity values were collected from one WO_2/C substrate.

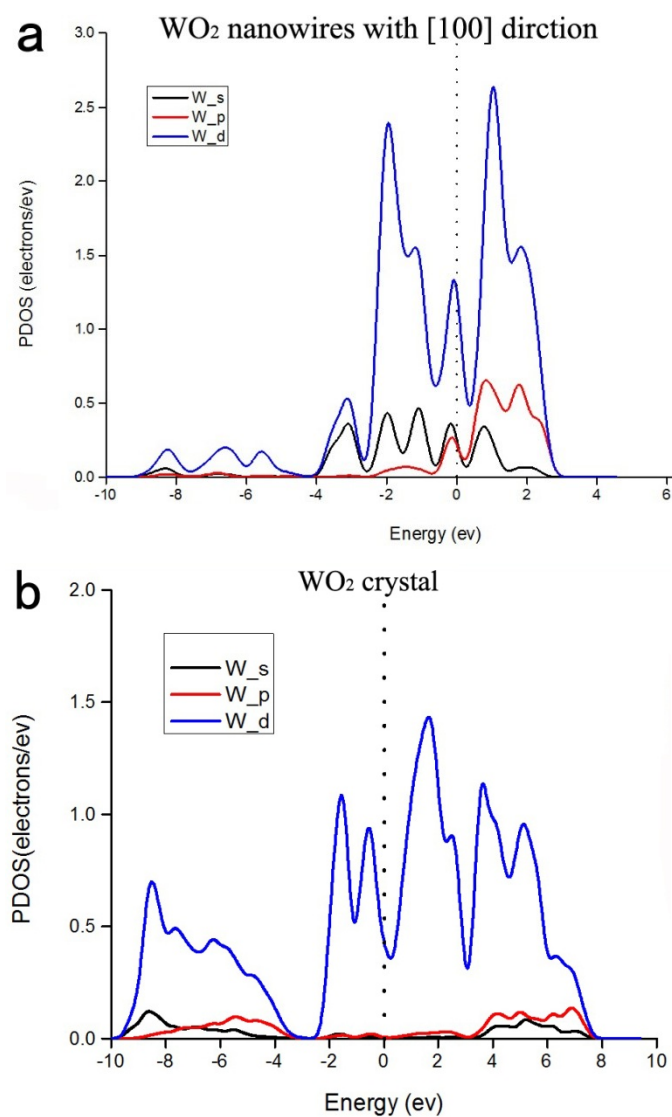


Figure S20. The PDOS of W atoms in WO_2 nanowires grown along the [100] directions and bulk crystal. Obviously, WO_2 nanowires grown along the [100] direction have more free electrons compared with bulk WO_2 .

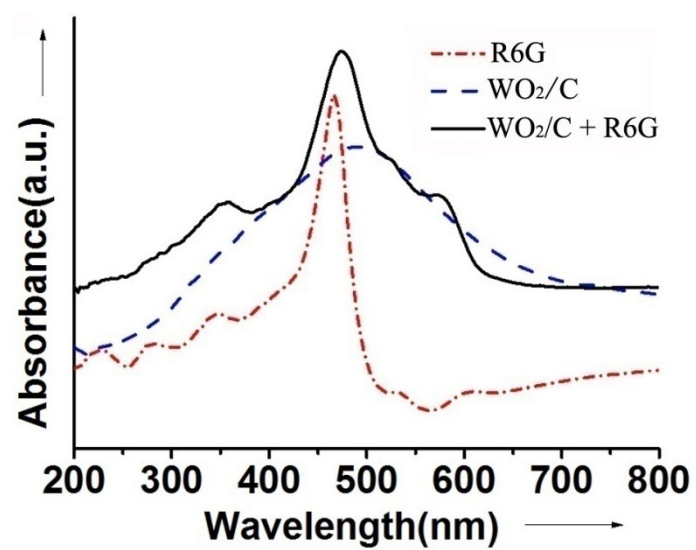


Figure S21. UV-Vis absorption spectra for R6G-modified WO₂/C compared with neat WO₂/C and R6G.

Table S1: Some of the Previously Reported EFs for Semiconductor Substrates

Material	Probe molecule	EF	Excited wavelength (nm)	Author
core-shell TiO ₂ -Ag	4-Mpy	6.5×10⁵	514	X. X. Zou et al. ^[1]
TiO ₂ photonic microarray	MB	2×10⁴	532	D. Qi et al. ^[2]
CdTe nanopartilces	4-Mpy	10⁴	514.5	Y. F. Wang et al. ^[3]
W ₁₈ O ₄₉ nanowires	R6G	3.4×10⁵	532.8	S. Cong et al. ^[4]
CuO nanoparticles	4-Mpy	10²	514.5	Y. Wang et al. ^[5]
CdS nanoparticels	4-Mpy	10²	514.5	Y. F. Wang et al. ^[6]
Cu ₂ O superstructure	R6G	8×10⁵	674	J. Lin et al. ^[7]
Fe ₂ O ₃ nanoparticles	4-Mpy	2.7×10⁴	514.5	X. Q. Fu et al. ^[8]
Au-CdSe nanowires	CV	10⁴	633	G. Das et al. ^[9]
Colloidal ZnO	D266	50	488	H. Wen et al. ^[10]
DFH-4T	MB	3.4×10³	785	Mehmet Yilmaz et al. ^[11]
TiO ₂	p-Nitrothio Phenol	10²	488	Teguh et. al. ^[12]
ZnO nanorods	4-ABT	22	514.5	Kim et. al. ^[13]
InAs/GaAs quantum dots	Pyridine	10³	514.5	Quagliano et. al. ^[14]
H-Si nanowire	R6G	8-28	532	Wang et. al. ^[15]
Graphene	Phthalocya	2-17	632.8	Ling et. al. ^[16]

	nine			
GaP	CuPc	700	514.5	Hayashi et. al. ^[17]
WO₂	R6G	1.3×10⁶	532	This work

- [1] X. X. Zou, R. Silva, X. X. Huang, J. F. Al-Sharab, T. Asefa, *Chem. Commun.* **2013**, 49, 382.
- [2] D. Qi, L. Lu, L. Wang, J. Zhang, *J. Am. Chem. Soc.* **2014**, 136, 9886-9889.
- [3] Y. F. Wang, J. H. Zhang, H. Y. Jia, M. J. Li, J. B. Zeng, B. Yang, B. Zhao, W. Q. Xu, *J. Phys. Chem. C*. 2008, 112, 996–1000.
- [4] S. Cong, Y. Y. Yuan, Z. G. Chen, J. Y. Hou, M. Yang, Y. L. Su, Y. Y. Zhang, L. Li, Q. W. Li, F. X. Geng, Z. G. Zhao, *Nat. Commun.* **2015**, 6, 7800.
- [5] Y. Wang, H. Hu, S. Jing, Y. Wang, Z. Sun, B. Zhao, C. Zhao, J. R. Lombardi, *Anal. Sci.* 2007, 23, 787–791.
- [6] Y. F. Wang, Z. H. Sun, Y. X. Wang, H. L. Hu, B. Zhao, W. Q. Xu, J. R. Lombardi, *Spectrochimica. Acta. Part. A*. 2007, 66, 1199–1203.
- [7] J. Lin, Y. Shang, X. X. Li, J. Yu, X. T. Wang, L. G. *Adv. Mater.* **2017**, 29, 1604797.
- [8] X. Q. Fu, F. L. Bei, X. Wang, X. J. Yang, L. D. Lu, *J. Raman Spectrosc.* **2009**, 40, 1290–1295.
- [9] G. Das, R. Chakraborty, A. Gopalakrishnan, D. Baranov, E. D. Fabrizio, R. Krahne, *J Nanopart Res.* **2013**, 15, 1596.
- [10] H. Wen, T. J. He, C.Y. Xu, J. Zuo, F. C. Liu, *Molecular Physics*. 1996, 88, 281–290.

- [11] M. Yilmaz, E. Babur, M. Ozdemir, R. L. Giesecking, Y. Dede, U. Tamer, G. C. Schatz, A. Facchetti, H. Usta, G. Demire, *Nat. Mater.* **2017**, DOI: 10.1038/NMAT4957.
- [12] J. S. Teguh, F. Liu, B. Xing, E. K. L. Yeow, *Chem. Asian J.* **2012**, 7, 975.
- [13] K. Kim, K. L. Kim, K. S. Shin, *Phys. Chem. Chem. Phys.* **2013**, 15, 9288.
- [14] L.G. Quagliano, *J. Am. Chem. Soc.* **2004**, 126, 7393.
- [15] X. Wang, W. Shi, G. She, L. Mu, *J. Am. Chem. Soc.* **2011**, 133, 16518.
- [16] X. Ling, L. Xie, Y. Fang, H. Xu, H. Zhang, J. Kong, Mi. S. Dresselhaus, J. Zhang, Z. F. Liu, *Nano Lett.* **2010**, 10, 553.
- [17] S. Hayashi, R. Koh, Y. Ichiyama, K. Yamamoto, *Phys. Rev. Lett.* **1988**, 14, 1085.